Published in Nukleonika, Vol. 21, No. 1, 3 - 28, (1976)

GEOMETRICAL PROPERTIES OF NUCLEI

William D. Myers

September 1975

Prepared for the U. S. Energy Research and Development Administration under Contract W-7405-ENG-48

DISCLAIMER

NUKLEONIKA — VOL. 21—No. 1/76

William D. Myers

*Lawrence Berkeley Laboratory***
University of California
Berkeley, California 94720
and
Institut für Kernphysik
Technische Hochschule Darmstadt
Darmstadt, West-Germany

GEOMETRICAL PROPERTIES OF NUCLEI*

Material concerning the geometrical properties of nuclei is drawn from a number of different sources. The leptodermous nature of nuclear density distributions and potential wells is used to draw together the various geometrical properties of these systems and to provide a unified means for their description. Extensive use is made of expansions of the radial properties in terms of the surface diffuseness. A strong case is made for the use of convolution as a geometrical ansatz for generating diffuse surface distributions because of the number of simplifications that arise which are of practicat importance.

Contents

* Work supported by the U.S. Atomic Energy Commission and the German Bundesministerium für Forschung und Technology

** Permanent address

I. Introduction

My main purpose in giving these lectures is to present a unified approach for dealing with many of the geometrical properties of nuclei. The basic assumption underlying the work is that a nucleus is a saturating system, i.e. characterized by a central region of approximately uniform density and having a total binding energy proportional to the number of particles (except for surface effects). For such systems simple relationships exist which allow many of the geometrical properties to be referred back to the single fundamental constant r_0, which is related to the density ϱ_0 of uniform (uncharged) nuclear matter by the expression $\varrho_0 = \left(\frac{4}{3}\pi r_0^3\right)^{-1}$.

The diffuse surface, which provides the transition from the approximately uniform interior to the outside vacuum, constitutes a substantial part of even the heaviest nuclei. Its width b (defined later) is the essential quantity entering the expressions which link together the various geometrical properties of the system. However, we shall see that for many purposes the nuclear density distribution may be treated as if the surface were sharp ($b = 0$). The actual properties of the diffuse distribution are either identical to those of the sharp distribution or very simply related to them.

The material I will present comes from a number of different sources. The first few sections are from work currently in progress by Swiatecki, Tsang, Randrup and others [1, 2]. The sections after that are taken directly from some earlier work of my own [3], which is in turn based on an unpublished work by Süssmann [4], and the last few sections are more recent results along similar lines. An important part of the proof given in Appendix A was pointed out to me by Zeldes, and the result obtained in Appendix B, was first suggested by Nix.

II. Definition of a Leptodermous System

The word "leptodermous", like a number of other words used in nuclear physics, (such as nucleus, or fission) has been taken from the field of biology. It is an adjective meaning "having a thin skin". One difference is that we use the word here in the relative rather than the absolute sense. Consequently, even elephants (called pachyderms because of their thick skins) are leptodermous in our usage. Perhaps an appropriate antonym would be "holodermous", meaning "all skin", a term that would apply, for example, to the lightest nuclei or to the electron distribution in atoms.

If the particle density of a system is given by $\varrho(\bar{r})$ and the local energy per particle by $e(\bar{r})$ then the energy density is $e\varrho$. (Note that no classical or statistical assumptions are

necessary. The quantities ϱ and $e\varrho$ could simply be the expectation values of the density and energy density operators.) The energy of the system is given by

$$E = \int e\varrho, \tag{1}$$

and this can be trivially rewritten as

$$E = Ae_1 + \int (e - e_1)\varrho. \tag{2}$$

We will define the system as "leptodermous" if a constant e_1 can be found so that the integrand in the second term is confined to a region in the surface which is small compared to the dimensions of the system.

For such a system, it is not difficult to show [1] that the total energy can be written as

$$E = E_{\text{bulk}} + E_{\text{surface layer}} + \text{terms of order}\left(\frac{\text{thickness of surface}}{\text{size of the system}}\right) \tag{3}$$

where

$$\begin{aligned} E_{\text{bulk}} &= e_1 A \\ E_{\text{surface layer}} &= c_2 S + c_3 K + c_4 G + c_4' Q. \end{aligned} \tag{4}$$

In this last expression, the quantities C_i are coefficients which may depend on the bulk density, but are independent of the shape of the system. The shape dependence enters thru the other quantities which are defined by the expressions:

$$\begin{aligned} S &= \int d\sigma, \quad \text{surface area,} \\ K &= \int \mathcal{K}\, d\sigma, \quad \text{integrated curvature,} \\ G &= \int \Gamma d\sigma, \quad \text{integrated Gaussian curvature,} \\ Q &= \int \mathcal{K}^2 d\sigma, \quad \text{integrated squared curvature.} \end{aligned} \tag{5}$$

These integrals are over the surface of the system. The symbol $\mathcal{K}$ represents the total curvature ($\mathcal{K} = R_1^{-1} + R_2^{-1}$) and Γ is the Gaussian curvature ($\Gamma = (R_1 R_2)^{-1}$), where R_1 and R_2 are the principal radii of curvature at that point.

This expansion only applies if the shapes being considered are not too contorted. For example, the expansion (4) would apply to the self energies of two colliding heavy ions, but not to the interaction energy between them. However, for two gently curved surfaces a somewhat similar treatment is possible in terms of the local properties at the point of of closest approach.

III. Proximity Force Theorem

As was pointed out in the previous section the leptodermous expansion, no matter how accurately done, is incapable of dealing with the interaction energy of two approaching objects. This problem, which is of primary interest in heavy-ion reactions, has been delt with in a variety of ways by various authors [5–11]. An alternative approach has been

developed by Randrup, Swiatecki and Tsang [2]. They have found it possible to derive a simple expression for the interaction energy between nuclei in terms of the interaction between flat surfaces of nuclear matter. Their method is quite general and applies not only to nuclei but to the interaction of two gently curved surfaces of any material whatever, whether of macroscopic or microscopic dimensions. The precise statement of the Proximity Force Theorem is that;

> "Under certain assumptions (having to do with keeping the density profiles of the two objects fixed), the *force* $F(s)$ between curved surfaces, as a function of the separation distance s, is proportional to the *potential per unit area* $e(s)$ between two flat surfaces, the proportionality factor being a certain mean radius of curvature characterizing the space between the two surfaces at the point of closest approach".

To establish the theorem consider the approach of two undeformable, spherical objects which are large with respect to the range of the interaction force. (The theorem is discussed in more generality in ref. 2). The total interaction energy can be written as an integral over the interaction energies of the individual surface elements facing each other a distance D apart, where D is a function of position in the gap separating the objects.

$$V_P = \int_{\text{gap}} e(D)d\sigma + \text{corrections}. \tag{6}$$

For the special case chosen here, the gap distance D is a function only of the radial distance r from the symmetry axis according to the expression

$$D(r) = s + \frac{1}{2}\left(\frac{1}{R_1} + \frac{1}{R_2}\right)r^2 + \ldots, \tag{7}$$

where s is the distance of closest approach and R_1 and R_2 are the radii of the two spherical objects. This expression can be written,

$$D(r) = s + \frac{1}{2}r^2/\bar{R}, \tag{8}$$

where $\bar{R}$ is the "reduced radius" characterizing the system defined by

$$\bar{R} = \frac{R_1 R_2}{R_1 + R_2}. \tag{9}$$

Returning to eq. (6) we can write

$$V_P(s) = \int_0^\infty e(D)2\pi r dr \tag{10}$$

or by substituting $dD = rdr/\bar{R}$ from (8) and noting that $D = s$ when $r = 0$ we have,

$$V_P(s) = 2\pi\bar{R}\int_s^\infty e(D)dD. \tag{11}$$

In eqs. (10) and (11) the integration has been extended to infinity; the precise upper limit doesn't matter if the interaction function $e(D)$ approaches zero sufficiently rapidly for large values of D.

The force acting between the two objects is given by

$$F_P(s) = -\frac{d}{ds}V_P(s) = 2\pi\bar{R}e(s) \tag{12}$$

proving the theorem cited earlier.

Note that the *force* between the objects is proportional, not to the *force per unit area* between flat surfaces, but rather it is proportional to the *interaction energy per unit area*.

If one has a model for semi-infinite nuclear matter then the function $e(s)$ can be calculated. This is done in ref. 2 and analytic approximations are given so the force (and consequently the interaction energy) of any two colliding nuclei can be calculated as the product of a proportionality factor $2\pi\bar{R}$ (where $\bar{R}$ brings in the size of the nuclei) and a single, known, universal function of distance $e(s)$.

Even without any model we can note that two semiinfinite surfaces are expected to attract each other until their effective sharp surfaces coincide $s = 0$. The energy gained at that points is 2γ, $e(0) = -2\gamma$, where γ is the surface energy per unit area, since a uniform density distribution throughout space is created when the two surfaces meet.

If the surfaces begin to interpenetrate there begins to be a region of double density in the overlap region and the energy rises because of compressibility effects. Consequently the maximum force between to colliding nuclei is when $s = 0$ and its value is

$$F_P^{\max} = F_P(0) = -4\pi\bar{R}\gamma \tag{13}$$

This equation expresses the remarkable result (see also ref. 10) that the maximum attraction between undeformable, gently curved bodies may be written down approximately without any knowledge of the nature of the cohesive interactions between the particles constituting the bodies, providing the surface energy is known.

IV. Geometrical Preliminaries

A. Leptodermous Distributions

The discussion of radial geometric properties of nuclei (here assumed to be spherical) is most easily carried out in terms of the quantities:

C, the "central radius",
R, the "equivalent sharp radius",
Q, the "equivalent r.m.s. radius" and
b, the "surface width". (14)

It is essential for the clarity of the following discussions that the definitions of these quantities and the relations between them be precisely understood.

The central radius C and the surface width b are the integral counterparts of the punctual quantities:

$R_{1/2}$, the half-value radius, and
t_{10-90}, the 10–90% distance. (15)

They are defined in terms of linear moments (as opposed to spherical moments) of the derivative of the normalized $f(0) = 1$ distribution function. If (as illustrated in Fig. 1) $f(r)$ is the distribution of interest, then

$$C = \int_0^\infty g(r) r\,dr,$$

$$b^2 = \int_0^\infty g(r)(r-C)^2 dr, \tag{16}$$

$$\int_0^\infty g(r)\,dr = 1,$$

where the surface distribution function $g(r)$ is defined by the expression

$$g(r) = -df(r)/dr. \tag{17}$$

The quantities C and b are the first two moments of the distribution $g(r)$. In a similar way additional information about the surface is available from higher moments such as the skewness and the kurtosis of this distribution, which can be obtained from Γ_3 and Γ_4, respectively, where

$$\Gamma_n = \int_0^\infty g(r)\,(r-C)^n dr. \tag{18}$$

This approach to the characterization of leptodermous distributions has been brought to a high degree of refinement by Süssmann [4], and the notation used here closely follows his.

For the commonly used Fermi distribution function

$$f(r) = 1/\{1+\exp[(r-c)/z]\}, \tag{19}$$

the quantities C, $R_{1/2}$, b, and t_{10-90} are related to c and z (for $e^{-c/z} \ll 1$) by the expressions

$$\begin{aligned} C &= R_{1/2} = c, \\ b &= (\pi/\sqrt{3})\cdot z, \\ t_{10-90} &= (2\ln 9)\cdot z. \end{aligned} \tag{20}$$

The next quantity of interest is the equivalent sharp radius R. It is defined here as the radius of a uniform sharp distribution having the same value in the bulk and the same volume integral as $f(r)$, i.e.,

$$\frac{4}{3}\pi R^3 f(\text{bulk}) = 4\pi \int_0^\infty f(r) r^2 dr. \tag{21}$$

For smooth leptodermous distributions (such as a Fermi distribution) the bulk value corresponds very closely to the central value and to this approximation $f(0)$ can be substituted for $f(\text{bulk})$ in eq. (21). Of course, for distributions that are leptodermous except for some smooth oscillations in the interior (for example, nuclear density distributions found in shell model or Hartree-Fock calculations) the punctual value $f(0)$ is clearly inadequate for the definition of R and some suitable average bulk value must be employed.

The final quantity of interest is the equivalent root-mean-square radius Q, which is defined by the expression

$$Q^2 = \frac{5}{3}\langle r^2 \rangle, \tag{22}$$

where

$$\langle r^n \rangle = \int_0^\infty r^n f(r) r^2 dr \Big/ \int_0^\infty f(r)\, r^2 dr. \tag{23}$$

The quantity Q is the special case for $k = 2$ of the quantity

$$R_k = \left[\frac{k+3}{3}\langle r^k \rangle\right]^{1/k}, \tag{24}$$

of Ford and Wills [12].

Of the three quantities C, R, and Q, the quantity of fundamental geometric importance is the equivalent sharp radius R. A sharp sphere having this radius is in a basic sense representative of the distribution $f(r)$. If the uniform central density of such a sharp sphere is set equal to the bulk value of $f(r)$, as defined in connection with eq. (21), then this sphere has the same volume integral as $f(r)$ and it differs from $f(r)$ *only in the surface region* (namely in the degree of diffuseness). The quantity C is mainly of interest bacause $R_{1/2} = C$ for the symmetric surface functions (such as Fermi distributions) often employed to characterize nuclear densities and potential wells. The quivalent r.m.s. radius Q is of interest since it is expected that this is the property of the distribution that is measured in some experiments [12, 13]. As can be seen in Fig. 1, sharp spheres with the same volume integral as $f(r)$ having the radii C or Q grossly misrepresent the appearance of the function $f(r)$, since they substantially differ from it over the bulk region.

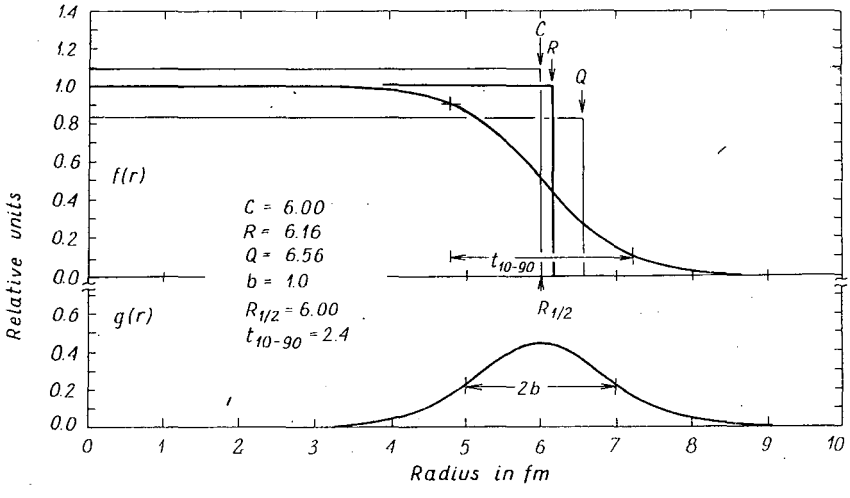

Fig. 1. The normalized, spherically symmetric, leptodermous distribution $f(r)$ and the corresponding surface distribution-function $g(r)$ are plotted against the radial distance r. The values of $R_{1/2}$ and t_{10-90} are given for this distribution in addition to the values of C, R, Q, and b whose use is advocated here. Sharp density distributions having the same volume integral as $f(r)$ and radii equal to C, R, and Q have also been drawn in for the purpose of demonstrating the geometrical importance of R

Süssmann has given exact expressions relating C and Q to R in terms of b and higher order moments of the surface [4]. However, the following approximate expressions suffice for most applications, and serve as simple reminders of the relationships of these quantities to each other:

$$C = R[1-\beta^2+\ldots],$$
$$Q = R\left[1+\frac{5}{2}\beta^2+\ldots\right], \tag{25}$$

where

$$\beta = b/R. \tag{26}$$

The range of applicability of these simple relationships can be seen in Fig. 2 where the ratios C/R and Q/R have been plotted against β^2 for a Fermi distribution. The solid straight lines correspond to the approximate predictions of eqs. (25) and the dashed lines to the

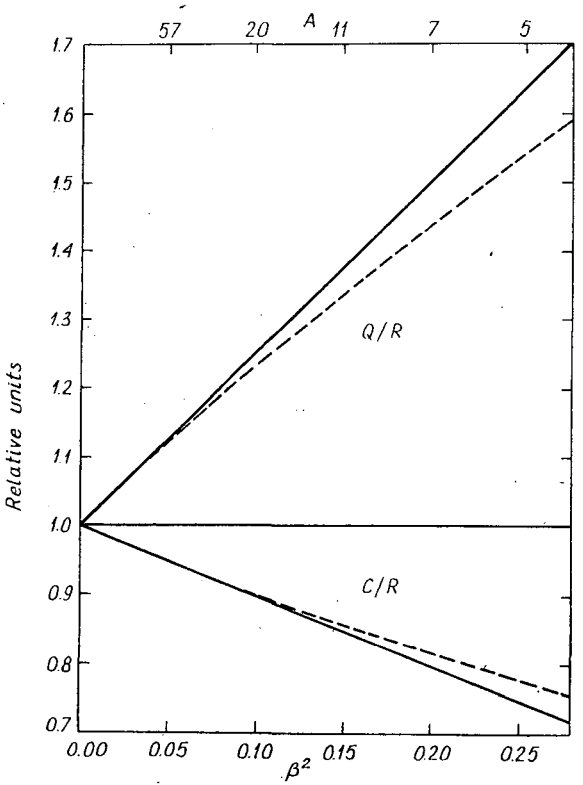

Fig. 2. The dashed lines plotted against β^2 represent the quantities Q/R and C/R for a Fermi function, and the solid lines represent the predictions of eqs. (25). The upper scale gives the corresponding nuclear mass number

actual values. At the top of the figure the approximate nuclear mass number is plotted corresponding to the assumption that nuclear density distributions can be represented by Fermi-distributions with $R = 1.16\ A^{1/3}$ and $b = 1.0$. We can see from this scale that

eqs. (25) are expected to be accurate to within 1% for C and 5% for Q all the way down to mass number $A = 9$. They are considerably more accurate over the bulk of the periodic table.

The relationship of C and Q to the more fundamental quantity R can be seen by referring back to Fig. 1. In this figure a Fermi distribution with $R_{1/2} = 6.00$ fm and $t_{10-90} = 2.4$ fm has been chosen to illustrate the geometric principles just described. The surface distribution function $g(r)$ has its first moment C — identical to $R_{1/2}$ in this case — and second moment b indicated in the figure. The radius R of the sharp sphere representing the function $f(r)$ is shown, as is the radial location corresponding to the value of Q. In any discussion of the geometric properties of this system, interest should focus on the equivalent sharp sphere whose radius is R and on the value of the surface thickness b. Other geometric properties that may be of interest can then be obtained from eqs. (25) or similar expressions.

B. Distributions Related by Convolution

There is a second distinct class of geometrical relationships in addition to the ones ust discussed that is also of considerable interest. These relationships connect the geometrical properties of one leptodermous distribution to the corresponding properties of a second distribution which is obtained from the first by folding in a function of short range. One example is a nuclear charge distribution obtained by folding the proton charge distribution into the assumed spatial distribution of the protons. Another example is a single-particle or optical model potential well obtained by folding a two-body interaction into the nuclear density distribution.

If the first distribution is $f_1(\bar{r}_1)$ and the folding (or convolution) function is $f_c(\bar{r}_{12})$, then the second distribution $f_2(\bar{r}_2)$ is defined by

$$f_2(\bar{r}_2) = \int d\bar{r}_1 \, f_1(\bar{r}_1) f_c(\bar{r}_{12}). \tag{27}$$

Probably the best known expression relating the geometric properties of f_1 and f_2 is

$$\langle r^2 \rangle_2 = \langle r^2 \rangle_1 + \langle r^2 \rangle_c. \tag{28}$$

Substitution of eq. (22), which relates Q and $\langle r^2 \rangle$, into eq. (28) results in the expression

$$Q_2^2 = Q_1^2 + \frac{5}{3}\langle r^2 \rangle_c. \tag{29}$$

Another useful relationship that can be easily established with the aid of eqs. (25) and (32) is

$$b_2^2 = b_1^2 + b_c^2 + \text{terms of order } \beta^2, \tag{30}$$

where the "width" b_c of the folding function has the special definition

$$b_c^2 = \frac{1}{3}\langle r^2 \rangle_c. \tag{31}$$

Since the expression relating the values of Q_1 and Q_2 shows that $Q_2 > Q_1$ in correspondence with one's intuition that f_2 should somehow be bigger than f_1, it may come as a sur-

prise that the equivalent sharp radii R_1 and R_2 are equal for leptodermous distributions where $\beta \ll 1$.

This result follows directly from the fact that the volume integral of f_2 is equal to the product of the volume integrals of f_1 and f_c. The easiest way to establish the relationship between R_1 and R_2 is to consider a normalized leptodermous function f_1 (where $f_1(\text{bulk}) = 1$) and a folding function f_c whose volume integral is unity. In such a case f_2 will also be normalized ($f_2(\text{bulk}) = 1$) and have the same volume integral as f_1. Then from the definition of R in eq. (21) it is easy to see that

$$R_1 = R_2, \text{ when } \beta \ll 1. \tag{32}$$

Equations (25), (26), (30), and (32) can be combined to give the following set of relations between the geometric properties of f_1 and f_2, which hold for $\beta_2 \ll 1$:

$$\begin{aligned} C_2 &= C_1(1-\beta_c^2+ \ldots), \\ R_2 &= R_1, \\ Q_2 &= Q_1\left(1+\frac{5}{2}\beta_c^2+ \ldots\right). \end{aligned} \tag{33}$$

These expressions show that when a short-range function is folded into a leptodermous distribution, another distribution is obtained that has a larger equivalent r.m.s. radius Q, and identical equivalent sharp radius R, and a central radius C that is smaller than the values of the corresponding quantities for the initial distribution.

V. Experimental Nuclear Density Distributions

The geometrical considerations of the previous section, which apply to any leptodermous distribution, are especially useful in the interpretation of experimental measurements of nuclear density distributions. They permit one to extract from these experiments an estimate of the equilibrium density ϱ_0 of neutral (all electromagnetic effects ignored), symmetric ($\varrho_n = \varrho_z$) nuclear matter. The quantity r_0 (a fundamental constant of nuclear physics) can then be calculated from the relationship

$$\varrho_0 = \left(\frac{4}{3}\pi r_0^3\right)^{-1}. \tag{34}$$

If nuclear matter were incompressible and nuclei had bulk neutron and proton densities in the ratio N/Z, then the equivalent sharp radii R_n and R_z of the neutron and proton distributions would be equal and proportional to $A^{1/3}$ with a proportionality constant equal to r_0, i.e.,

$$R_n = R_z = r_0 A^{1/3}. \tag{35}$$

Of course, this simple relationship is not expected to hold exactly because nuclear matter is not completely incompressible. Small deviations are expected — for example, see refs. 14–18 — because the surface energy tends to squeeze the nucleus to a smaller radius, and both the Coulomb energy and the loss of cohesion due to excess neutrons cause the nucleus to dilate to a larger radius. Since the relative importance of these effects varies through

the periodic table, some nuclei are smaller and some larger than is predicted by eq. (35). Another effect of the excess neutrons is the creation of a neutron skin.

Consequently, not only does the average radius R_ϱ differ from eq. (35), but the separate neutron and proton radii (R_n and R_z) differ from R_ϱ and from each other. The expressions relating these quantities are

$$R_\varrho = (NR_n + ZR_z)/A, \qquad R_n = R_\varrho + \left(\frac{Z}{A}\right) t,$$

and (36)

$$t = R_n - R_z, \qquad R_z = R_\varrho - \left(\frac{N}{A}\right) t,$$

where the effective sharp radius of the matter distribution R_ϱ is the weighted average of R_n and R_z and t is the neutron skin thickness. [See ref. 15].

It should be noted that even if nuclear matter were incompressible and R_n and R_z were strictly proportional to $A^{1/3}$, the quantities C and Q would not [as can be seen in eqs. (25)] be simply proportional to $A^{1/3}$. In spite of this, attempts are often made to establish such relationships. Exceptions to this erroneous approach are to be found in a number of places such as refs. 19 and 20 where Elton makes use of expressions similar to eqs. (25) (but specialized to Fermi distributions and taken to higher order) to relate C and Q to the more fundamental quantity R.

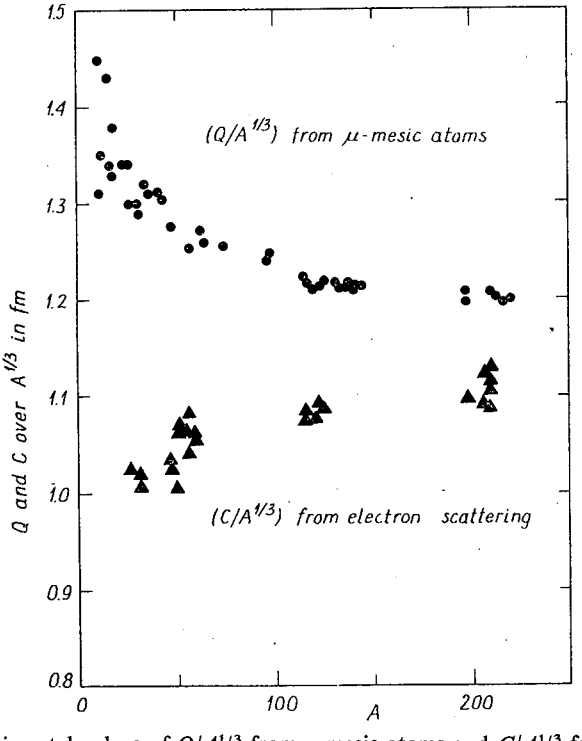

Fig. 3. A plot of experimental values of $Q/A^{1/3}$ from μ-mesic atoms and $C/A^{1/3}$ from electron scattering against mass number A for nuclei throughout the periodic table [19]

Figure 3 shows what happens when the ratio of C or Q to $A^{1/3}$ is plotted against A for nuclei throughout the periodic table. The data points, which are all from ref. [19], are represented by circles when they are based on Q values from μ-mesic atom experiments and by triangles when they are based on C (or $R_{1/2}$) values from election scattering. The reason for listing the C values for electron scattering is that this quantity and the quantity b are the properties of the nuclear charge distribution that are determined (to lowest order in β^2) by the experiments [21]. Similarly, the quantity Q is plotted for the μ-mesic atom experiments because it is the one actually determined [12]. While the $Q/A^{1/3}$ values are not exactly constant they do seem to tend to an asymptotic value of about 1.2 fm, and the $C/A^{1/3}$ values seem to tend to approximately 1.1 fm. The numbers obtained in this way are often erroneously assumed to correspond to the fundamental constant r_0 defined in eq. (34).

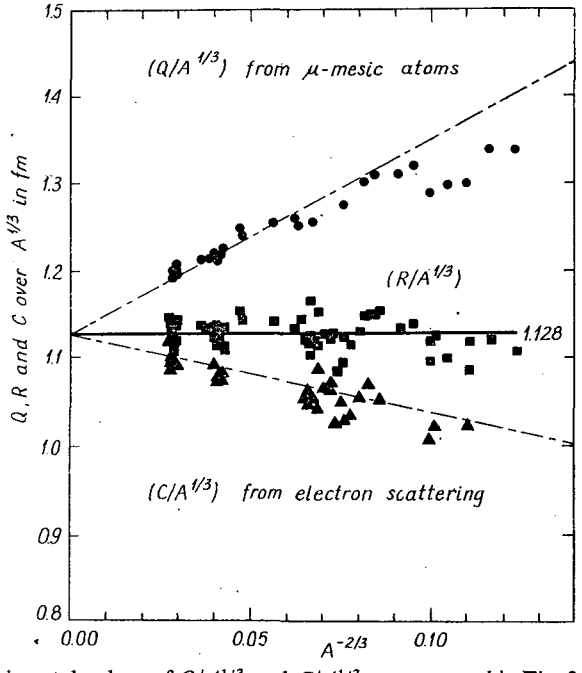

Fig. 4. The same experimental values of $Q/A^{1/3}$ and $C/A^{1/3}$ as were used in Fig. 3 are plotted here against $A^{-2/3}$. The values of $R/A^{1/3}$ for these experimental points are also plotted and are seen to scatter about the solid horizontal line at 1.128 fm. The corresponding predictions for $Q/A^{1/3}$ and $C/A^{1/3}$ are given as dot-dashed lines

That there is no discrepancy between the two different types of measurements is easily seen in Fig. 4. If R_z were nearly proportional to $A^{1/3}$ then eqs. (25) could be rewritten in the form

$$\begin{aligned} C_z/A^{1/3} &\approx a[1-(b/a)^2 A^{-2/3}+\ldots], \\ R_z/A^{1/3} &\approx a, \\ Q_z/A^{1/3} &\approx a\left[1+\frac{5}{2}(b/a)^2 A^{-2/3}+\ldots\right]. \end{aligned} \tag{37}$$

These expressions lead us to expect straight lines (in the limit of $A^{-1/3} \ll 1$) when the experimental ratios of C and Q to $A^{1/3}$ are plotted against $A^{-2/3}$. In Fig. 4 we see that this expectation is fulfilled and that the data, except for the lightest nuclei, are consistent with straight lines having a common intercept at

$$a = 1.128 \text{ fm}, \tag{38}$$

and slopes corresponding to

$$b = 1 \text{ fm}. \tag{39}$$

According to eqs. (20), this implies a value for t_{10-90} of 2.4 fm for a Fermi distribution. In this figure the solid squares represent values of $R_z/A^{1/3}$ determined from the C_z and Q_z values by inverting eqs. (12). The figure shows that this quantity is in fact nearly independent of nuclear size.

If nuclear matter were strictly incompressible and if the equivalent sharp radii of the neutrons and protons (R_n and R_z) were identical, then the fundamental constant r_0 would have the same value as the proportionality constant (1.128 fm) determined above. The actual, more complex, relationship between these quantities has been investigated with the droplet model of nuclei which includes such important effects as compressibility and the influence of the neutron excess on the creation of a neutron skin [14, 15].

A. Droplet Model Considerations

In order to estimate the value of r_0 from determinations of C and Q for the proton distribution it is first necessary to convert these quantities to R_z (the effective sharp radius of the protons) as was done in the previous section. The value of R_z can then be related to r_0 by means of a macroscopic model that includes compressibility effects and the possible existence of a neutron skin. Of course, selfconsistant calculations (using the Hartree-Fock or Thomas-Fermi approximations) include these effects automatically but require rather elaborate calculations in which the physical origin of the effects is lost. Alternatively, one can make use of the Droplet Model expressions for R_ϱ and t which are

$$\begin{aligned} R_\varrho &\approx r_0 A^{1/3}(1+\bar{\varepsilon}), \\ t &\approx \frac{2}{3} R_\varrho (I-\bar{\delta}), \end{aligned} \tag{40}$$

where $\bar{\varepsilon}$ is a measure of the deviation of the central density of the nucleus from its nuclear matter value and $\bar{\delta}$ is the effective value of the nuclear asymmetry in the interior of the nucleus. These quantities are defined by the expressions

$$\begin{aligned} \bar{\varepsilon} &= -\frac{1}{3}\left(\frac{\varrho-\varrho_0}{\varrho_0}\right)_{\text{ave. over bulk}}, \\ \bar{\delta} &= \left(\frac{\varrho_n-\varrho_z}{\varrho}\right)_{\text{ave over bulk}}, \end{aligned} \tag{41}$$

and

$$I = (N-Z)/A.$$

The actual values of $\bar{\varepsilon}$ and $\bar{\delta}$ depend on the N and Z values of the particular nucleus and the values of the various coefficients entering the Droplet Model. Refs. [14–16, 22] should be consulted for further applications of the model.

Figure 5 (from ref. 22) shows how the fundamental constant r_0 is related to the equivalent sharp radius R_z of the proton distribution, for nuclei throughout the periodic table.

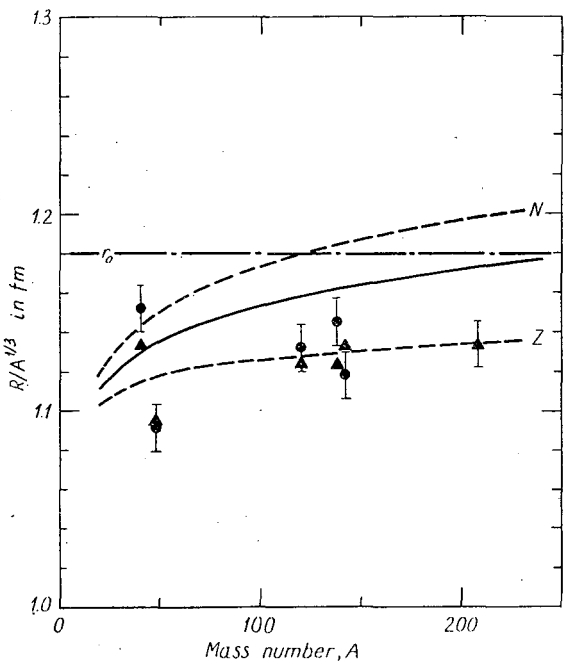

Fig. 5. Various quantities characteristic of the radial extent of spherical nuclei are plotted versus the mass number A. The dots with error bars represent the $R_z/A^{1/3}$ values for six different spherical nuclei and the associated triangles are the Droplet Model predictions for this quantity. The other lines, which represent $R_n/A^{1/3}$, $R_\varrho/A^{1/3}$ and $R_z/A^{1/3}$ predictions for nuclei along beta-stability are discussed in more detail in the text

In this figure the dashed lines labeled N and Z correspond to the droplet model predictions for the quantities $(R_N/A^{1/3})$ and $(R_Z/A^{1/3})$ for nuclei along the bottom of the valley of beta-stability. The solid line, which is the weighted mean of the neutron and proton lines represents the value of $(R_\varrho/A^{1/3})$ for the total nucleon density. The solid dots correspond to the experimental values of $(R_Z/A^{1/3})$ for various spherical nuclei. The error bars of $\pm .012$ fm were chosen to represent the spread in values observed in the tabulated results. Solid triangles indicate the droplet model value of $(R_Z/A^{1/3})$ for these same nuclei.

A dot-dashed line is drawn across the figure at 1.18 fm to indicate the value of r_0 that was used in the Droplet Model calculation. The solid line representing the average radius of the neutron and proton distributions lies below this value because finite nuclei are squeezed by the surface tension. This squeezing is gradually offset, as one moves toward heavier nuclei, by the Coulomb dilatation.

The dot-dashed lines showing the separate neutron and proton radii, R_n and R_z, show

the same trend with A as the total matter radius R_ϱ. In addition they spread further and further apart as the neutron skin thickness grows due to the increasing neutron excess with increasing values of A. The growth of this neutron skin (whose thickness is about 0.35 fm at $A = 200$) reduces the increase in $R_z/A^{1/3}$ with the consequence that this ratio is nearly constant throughout the periodic table. The value of $r_0 = 1.18$ fm was chosen for this calculation so the experimental and calculated radii for the proton distributions would agree.

We can conclude that the nuclear radius constant of standard nuclear matter can be inferred with considerable accuracy from the experimental results, which only determine the radius of the proton distribution R_z, and that it has the approximate value

$$r_0 = 1.18 \text{ fm}. \tag{40}$$

An uncertainty of perhaps $\pm 2\%$ should be assigned to this number because there is some model dependence in the way it is obtained. This is the value of r_0 that should be employed in nuclear matter calculations rather than the unwarranted choice of values like 1.10 fm or 1.20 fm that we discussed earlier in connection with Fig. 3.

The equivalent sharp radii of the proton distributions are given approximately by $A^{1/3}$ times the proportionality constant in eq. (38), 1.128 fm, or more precisely by performing the appropriate droplet model calculation with the value of r_0, 1.18 fm, given above. Once R is known then eqs. (25) can be used to make the simple geometrical corrections necessary to determine C and Q for comparison with experiment.

VI. Optical Model Potential Wells

The geometrical relationships given earlier, and employed in the last section for the interpretation of nuclear-density distributions, apply equally well to optical model potential wells. Indeed, the Woods-Saxon functional form of optical model wells is the same Fermi distribution as is used to describe nuclear densities. As regards geometrical properties the main difference between the optical model wells and the density distributions is that there is no reason to expect — even under the assumption of incompressibility — that the equivalent sharp radius of the potential R_v should be proportional to $A^{1/3}$.

A. Interpretation of Experiments

Many authors, unsatisfied with simply fitting potential well parameters to experiment, have cast about for some plausible scheme for correlating the resulsts obtained for different nuclei. The procedures that have come into common use, such as "fixed geometry fits" and various ways of deriving the potentials by folding an interaction into the density, all have serious deficiencies. The problems that arise when these methods are employed will be discussed below in connection with Fig. 6.

The three separate sections of Fig. 6 have been collected together because of their similarity, and to facilitate comparisons between one section and another as the discussion

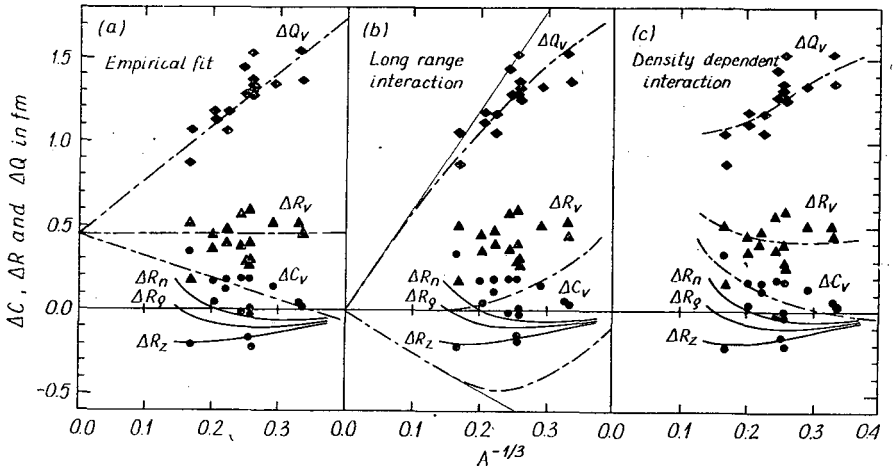

Fig. 6. The differences (signified by Δ) between the Q_v, R_v and C_v values of experimental optical model potentials and reference values equal to 1.16 $A^{1/3}$ fm are plotted against $A^{-1/3}$. Similarly the solid lines at the bottom of each section represent droplet-model predictions for the various matter radii. The dot-dashed lines represent three different ways of correlating the experimental information on the potential wells: (*a*) an empirical fit, (*b*) a fit obtained by folding a non-saturating force into empirical density distributions, (*c*) a fit obtained by folding a saturating force into the droplet model density distributions

progresses. After the features common to all three sections have been explained each separate section will be discussed in turn.

The experimental data consists of Woods-Saxon well parameters given in refs. 23, 24 for optical model fits to 40–60 MeV proton scattering on nuclei throughout the periodic table. Equations (20), (25), and (26) have been used to convert these parameters to values of Q_v, R_v, and C_v for each of the potential wells. (The subscript v means that these quantities refer to geometrical properties of the potential). Then the quantity 1.16 $A^{1/3}$ fm was subtracted from each of these numbers for the sole purpose of displaying, on an expanded scale, the relations between the different quantities.

The values actually plotted versus $A^{-1/3}$ in each section of the figure are ΔQ_v (as diamonds), ΔR_v (as triangles), and ΔC_v (as circular dots), where

$$\begin{aligned} \Delta Q_v &= Q_v - 1.16\ A^{1/3}, \\ \Delta R_v &= R_v - 1.16\ A^{1/3}, \\ \Delta C_v &= C_v - 1.16\ A^{1/3}. \end{aligned} \tag{41}$$

The heavy solid lines near the bottom of each section represent the values of ΔR_ϱ, ΔR_n, and ΔR_z obtained from a droplet model calculation of these quantities similar to the one discussed earlier in connection with Fig. 5) that was fitted to the experimental values of R_z. Since these lines represent the various nuclear density distributions and the experimental points represent various properties of the potential wells we might expect to learn a great deal from these figures about the relationships between them.

One of the first things one notices in Fig. 6 is that R_v is greater than R_ϱ by an almost constant amount throughout the periodic table. In fact, very close correspondence can

be seen in Fig. 6a between the experimental points and the dot-dashed lines that correspond to

$$R_v = 1.16\ A^{1/3} + 0.45 \text{ fm},$$
$$b_v = 1.3 \text{ fm}. \tag{42}$$

In the "fixed geometry fits" commonly employed for the interpretation of optical model data, the half-value radius $R_{1/2}$ is generally assumed to be proportional to $A^{1/3}$, and some suitable value is chosen for the proportionality constant so as to best reproduce data throughout the periodic table. The choice of the quantity $R_{1/2}$ for a parametrization of this kind is puzzling, since we showed earlier that a sharp sphere with the radius C_v does not serve to represent the corresponding distribution (recall that $R_{1/2} = C$ for Woods-Saxon wells). Moreover, there is no physical basis for assuming such proportionality for the potential well, even for the more fundamental quantity R_v. The main reason for constraining the fits in this way has been to force an apparent reduction in the uncertainty of the determination of the real and imaginary potential well depths. The trends in these quantities with increasing mass number and neutron excess are then considered to be significant, and physical interpretation of the results is sometimes attempted. It should, however, be clear by now that this whole procedure is questionable [see ref. 13 for other comments along this line], since the unjustified nature of the constraints probably introduces spurious trends into other quantities of interest.

B. Potentials Obtained by Folding

Other authors, unsatisfied with simply fitting well parameters to experiment or using empirical relations like eq. (42) to correlate their data, have employed optical potentials obtained from the nuclear density distributions by folding in a simple two-body interaction. To appreciate some of the problems that can arise when this is done it is necessary to recall the relations between the geometrical properties of such distributions as given in eqs. (33). These equations immediately bring one difficulty to our attention, since they show that R_v must equal R_ϱ, in direct disagreement with the experimental results shown in Fig. 6.

This discrepancy manifests itself in different ways in the two distinctly different approaches that have been taken. Some authors take the density distribution from electron scattering as given and fold in a rather long-range force to generate an optical potential that fits the experimental data. This method is considered in refs. 25, 26 along with a number of others. It results in a more diffuse potential than would be obtained in an optical model fit, but one which has approximately the same value for Q_v. [It has been found empirically that different potentials havign the same volume integral and the same equivalent r.m.s. radius Q_v give approximately the same predictions]. The values of the geometrical parameters R_v and b_v of the resulting potential differ substantially from the values that would be obtained for a Woods-Saxon well fitted directly to experiment. Other authors allow the density to vary in the fitting process and obtain potentials very similar to those found by fitting Woods-Saxon wells [13]. However, the geometrical pa-

rameters of the density distributions obtained differ substantially from those found in other experiments aimed directly at determining these distributions.

An example illustrating the first procedure mentioned above is shown in Fig. 6b. The dot-dashed lines plotted in this figure for Q_v, R_v, and C_v were calculated from optical model potential wells generated by first assuming a fairly realistic density distribution given by

$$\begin{aligned} R_\varrho &= 1.16\ \mathrm{A}^{1/3}\ \mathrm{fm}, \\ b_\varrho &= 1.0\ \mathrm{fm}, \end{aligned} \tag{43}$$

and folding in a Gaussian interaction of the form

$$f_g(r) = -V \exp -(r/a_g)^2 \tag{44}$$

with a range $a_g = 1.86$ fm chosen so the experimental values of Q_v are reproduced. The width, b_c, of this interaction is 1.32 fm since,

$$b_c = a_g/\sqrt{2}\,. \tag{45}$$

The long range part of the Hamada-Johnston potential, which is currently in vogue for the interpretation of proton-nucleus scattering data [see the discussion in refs. 25 and 26], has a width of about 1.4 fm and is quite similar to the interaction used here.

Equation (30) shows that the surface width b_v of the potentials resulting when (44) is folded into (43) is 1.65 fm. This is not a very satisfactory result since it is substantially larger than the 1.3 fm value obtained by simply fitting Woods-Saxon wells to experiment.

It should be pointed out in passing that if the potentials being considered in Fig. 6b were leptodermous, Q_v and C_v would lie on the thin straight lines predicted by eqs. (25) and R_v would be exactly zero. The reason the dot-dashed lines representing these quantities deviate is that the long range of the folding interaction produces potential wells so diffuse that they are no longer leptodermous for the smaller nuclei.

The other possible approach to the problem of generating optical potentials by folding is to vary both the radius of the density distribution and the range of the force. An extensive analysis of this type is contained in ref. 13. When this is done the optical model wells obtained have geometrical properties similar to those obtained by fitting Woods-Saxon wells [see eq. (42)]. Since $b_v \approx 1.3$ fm we can see from eq. (30) that b_c must be approximately 0.83 fm, which corresponds to a range $a_g = 1.17$ fm for a Gaussian interaction. Since $R = R_v$[from eqs. (33)] it is clear [from eq. (42)] that this fitting procedure must result in density distributions for which

$$R \approx 1.16\ A^{1/3} + 0.45\ \mathrm{fm}, \tag{46}$$

in substantial disagreement with what is known about this quantity. Unreasonably large density distributions are always obtained when this procedure is employed, simply because of the geometrical relations involved.

C. Density Dependent Interactions

It might have been anticipated that nuclear density distributions and optical model potential wells are not related in a way corresponding to the folding in of a simple two-body

interaction such as the one given in eq. (44). If any sort of self-consistent calculation of nuclear properties is attempted with such a force the system collapses. It is well known that the force employed in such calculations must become effectively weaker as the nuclear density increases so as to lead to saturation. This feature (the apparent decrease in interaction strength with increasing density) is just the feature needed to resolve the difficulties encountered in the optical model fits. Figure 7 shows the relationship between the density

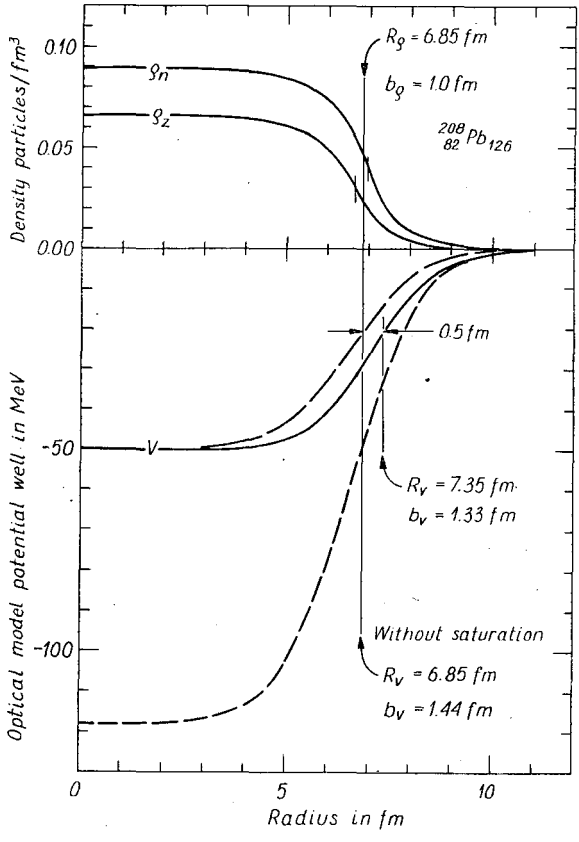

Fig. 7. Droplet model density distributions for $^{208}_{82}Pb_{126}$ are plotted against radial distance in the upper part of the figure. Short vertical bars on ϱ_n and ϱ_z indicate the location of the equivalent sharp radii R_n and R_z. The long vertical line indicates the location of the equivalent sharp radius of the total density R. This same line indicates the location of the equivalent sharp radius of the potential (obtained by folding the nonsaturation part of eq. (47) into the density) plotted in the lower part of the figure as a dashed line. The lower dashed line is the potential itself and the upper dashed line is the same curve normalized to the solid line which represents the potential obtained when the complete saturating interaction, eq. (47), is used. A shorter vertical line indicates the location of the equivalent sharp radius of this latter potential and shows that it lies substantially outside that of the non-saturation potential

distribution of $^{208}_{82}Pb_{126}$ and an optical model potential well obtained by folding in a saturating two-body interaction. The form of the interaction chosen for this example was

$$f_c(r) = -Ve^{-(r/a)^2}(1-c\varrho^{2/3}), \tag{47}$$

where

$$V = 51 \text{ MeV}.$$
$$a = 1.39 \text{ fm}, \tag{48}$$
$$c = 2 \text{ fm}^2.$$

In Fig. 7 the neutron and proton density distributions predicted by the droplet model are shown. Their equivalent sharp radii are indicated by short vertical bars. The equivalent sharp radius of the density R_ϱ (the sum of R_n and R_z) is shown as a long vertical line. As we know from eq. (32) the equivalent sharp radii are identical for the density and the potential generated from it with a simple interaction. Consequently, the same vertical line that locates R_ϱ also serves to locate R_v in the case (shown as the lower dashed line in the figure) where the interaction of eq. (47) is employed without the last factor. When we consider the solid curve where the entire interaction is used, including the last term with its density dependence, we see that the discrepancy that mars earlier attempts to relate experimentally determined densities and potential wells has disappeared. The solid curve labeled V in Fig. 7 approaches its bulk value more quickly than does the dashed curve, because the interaction generating it becomes effectively weaker towards the interior. Consequently, the equivalent sharp radius R_v of this potential well lies outside of R_ϱ, in agreement with experiment.

Since the potential well produced by the saturating interaction, eq. (47), is shallower everywhere than the corresponding potential well produced by the non-saturating part of the interaction it is possible to gain the impression from Fig. 7 that the non-saturating potential is larger (in some vague sense), even though the geometric fact is the reverse. To offset this illusion the dashed curve representing the non-saturating part of the interaction has been replotted as a second dashed curve having the same bulk value as the solid curve representing the potential produced by the complete interaction. In comparing these two curves (with the same bulk values) it is easier to see that the equivalent sharp radius R_v of the saturating potential lies 0.5 fm outside that of the non-saturating potential. Indeed, it is possible, in analogy with the proof of eq. (32), to establish the theorem that the equivalent sharp radius R_v of any potential well produced by a saturating interaction (i.e., the strength decreases with increasing density) is larger than that for a potential well produced by the non-saturating part of the same interaction.

It is necessary to refer back to Fig. 6 in order to see how the use of a saturating interaction improves the agreement with experimentally determined optical model potential wells throughout the periodic table. In Fig. 6c the dot-dashed lines represent the geometrical properties of the potentials obtained by folding the saturating interaction of eq. (47) into the density distributions predicted by the droplet model. Contrast the good agreement thus obtained with the rather poor agreement obtained in Fig. 6b with the use of a non-saturating interaction.

No special effort has been made to refine the choice of effective two-body interaction used here, since the main concern is with the purely geometrical aspects of the problem. In a more general study of the relation between optical model wells and nuclear properties, the energy and isospin dependence of the effective interaction would have to be considered, as well as effects due to antisymmetrization.

What we have shown is that nuclear density distributions and potential wells that have been deduced from experiment *cannot* be related satisfactorily by folding in a simple non-saturating two-body interaction for purely geometrical reasons. It is likely that any number of reasonable saturating interactions will be able to provide this connection whether they be non-local, density dependent, or velocity dependent.

VII. Convolution as a Geometrical Ansatz

In the last section it was pointed out that a number of problems arise when one attempts to generate optical model potential wells by folding a short range interaction into the density distribution. However, there are a number of applications where simple folding is an extremely useful approach. One of these applications concerns a modified definition of the liquid-drop model surface energy [5] that is free of the spurious sensitivity to high multipole wiggles in the shape of the drop which characterizes the usual approach. Another application whose significance is just beginning to be realized is the use of convolution as a geometrical ansatz for creating diffuse surface distributions. In virtually all of the literature of nuclear physics diffuse surface distributions (of density or potential) are represented by Fermi functions (like eq. (19)). This choice has a number of awkward features which are easily overcome by creating the diffuse distribution from one with a sharp surface by convolution.

A. Normalization

When a Fermi-function is used to represent a nuclear density distribution its volume integral must be chosen to contain the correct number of nucleons. This is not a simple task even for spherical nuclei. The integral must be done numerically and the half-radius c chosen by successive approximations. For a deformed nucleus this becomes a two or three-dimensional numerical integration and interaction procedure. (Or one can use analytic approximations of various kind if it isn't important to have the number of particles exactly right.) By contrast, the normalization problem completely disappears when the diffuse density distribution is generated by folding. The volume of a distribution generated by folding two other distributions together is the product of their separate volumes. If the convolution function is normalized to unit volume, then the diffuse surface function has the same volume as the sharp distribution it is derived from and no calculation whatever is required.

B. Multipole Moments

Another advantage of using convolution to generate diffuse surfaces is that the diffuseness normal to the surface is nearly the same at any point on the surface. This is true as long as the local curvature of the surface is not too great. When Fermi functions are used the diffuseness [the quantity b from eq. (16)] normal to the surface is proportional to the

cosine of the angle between the radius vector and a normal at that point. This kind of angular dependence of the surface diffuseness can generate spurious multipole moments that have no basis in reality.

Perhaps the most useful feature of diffuse distributions created by convolution is that their multipole moments are identical to the moments of the sharp-surfaced generating functions they are based on (see Appendix A). This means that only sharp distributions need be employed in the discussion of any physical phenomena that is concerned with multipole moments. Because of the identity of the moments; such a discussion applies equally well to diffuse distributions created by convolution. This is certainly not the case when Fermi-functions are used to create the diffuseness.

Papers have been written and tables of numerically calculated conversion factors have been compiled [27], for relating the multipole moments of a Fermi-function to those of the generating shape. Appendix A shows that the need for such conversions is not a general feature of diffuse distributions, but simply an artifact created by the poor choice of method for creating the diffuseness.

C. Moments of Inertia

A number of nuclear phenomena depend upon the moments of inertia of nuclei whose deformations are sometimes simple (nuclear ground states) and sometimes complex (fission barriers for example, or colliding heavy-ions). Questions often arise as to the effect of diffuseness on these phenomena which, up until now, have usually, been discused only in terms of sharp-surfaced density distributions. Of course, if Fermi-functions are used to create the diffuseness, numerical integrations would be required to calculate the conversion factors for every case of interest.

If convolution is used to create the diffuseness then the moments of inertia of the diffuse and sharp distributions are related by the simple expression,

$$I_2 = I_1 + 2\,Mb_c^2, \tag{49}$$

which is derived in Appendix B. In this expression I_2 is the moment of inertia of the diffuse distribution about an arbitrary axis and I_1 is the corresponding moment of inertia for the sharp-surfaced function it is derived from. The quantity M is the total mass of the object and b_c is the "width" of the convolution function, as defined by eq. (31).

Actually generating the density distribution itself (or the diffuse surface potential well) by folding may be complicated, depending on the generating shape. But, since one is usually interested in the properties of the distribution such as radial moments, multipole moments, moments of inertia, etc., it is often unnecessary to generate the distribution. If the diffuseness is thought of in terms of convolution as a geometrical ansatz, then only sharp distributions need actually be employed in the calculations.

VIII. Concluding Remarks

The purpose of these lectures was to provide a basis for the unified treatment of geometrical properties that are sometimes thought of as separate and distinct. The leptodermous

nature of nuclei provides the necessary unifying feature. The fact that the energy can be expanded in powers of the relative diffuseness was discussed first and then it was shown how similar methods can be extended to include an approximate treatment of nucleus-nucleus potentials in heavy-ion collisions. The simple geometrical relationships that hold between various radial properties were introduced and then extended to include the expressions that apply for distributions related by convolution. After showing how these relationships contribute to the analysis of experimental results on nuclear charge radii a brief diversion was made to show how the Droplet Model could be employed to determine r_0. A section was devoted to the pitfalls encountered when one tries to generate optical model potential wells by folding a simple two-body interaction into the nuclear density distribution. The final sections were devoted to illustrating the advantages of using convolution as a geometrical ansatz for generating diffuse distributions. It was shown that this method avoids many of the complications that arise when Fermi-functions are used.

Appendix A. — Multipole Moments

The multipole moments, defined by the expression

$$Q_l = \int \varrho(\bar{r}) r^l Y_{l0}(\hat{r}) d^3_{r_u} \tag{A1}$$

of two distributions $\varrho_1(r_1)$ and $\varrho_2(\bar{r}_2)$ are identical, for distributions which are related by convolution, according to the expression,

$$\varrho_2(\bar{r}_2) = \int \varrho_1(\bar{r}_1) f_c(|\bar{r}_2 - \bar{r}_1|) d^3_{r_1} \tag{A2}$$

where

$$\int f_c(s) d^3_s = 1 \tag{A3}$$

The equality of the moments for these distributions is easily established by noting that

$$Q_{l,1} = \int \varrho_1(\bar{r}_l) \bar{r}_1^l Y_{l,0}(\hat{r}_1) d^3_{r_1} \tag{A4}$$

and

$$Q_{l,2} = \int \Big[\int \varrho_1(\bar{r}_1) f_c(|\bar{r}_2 - \bar{r}_1|) d^3_{r_1} \Big] r_2^l Y_{l,0}(\hat{r}_2) d^3_{r_2} \tag{A5}$$

The latter expression can be rewritten as

$$Q_{l,2} = \int \varrho_1(\bar{r}_1) \Big[\int f_c(s) r_2^l Y_{l,0}(\hat{r}_2) d^3_s \Big] d^3_{r_1} \tag{A6}$$

where $\bar{s} = \bar{r}_2 - \bar{r}_1$ and the integration over $\bar{r}_2$ has been replaced by integration over $\bar{s}$. Since the average value of a harmonic function over the surface of a sphere is equal to its value at the center [28], the integral in the bracket can be rewritten as

$$\int f_c(s) 4\pi s^2 \cdot [r_1^l Y_{l,0}(\hat{r}_1)] ds \tag{A7}$$

where we have made use of the fact that $\bar{r}_1 = \bar{r}_2$, when $\bar{s} = 0$. The remaining integration is just the normalization integral for the convolution function (A3). So the bracket reduces to $r_1^l Y_{l,0}(\hat{r}_1)$, which when substituted into (A6) gives an expression identical to (A4) proving the theorem.

Appendix B. — Moments of Inertia

The moments of inertia I about any axis of two density distributions $\varrho_1(\bar{r}_1)$ and $\varrho_2(\bar{r}_2$ related by convolution (as in the previous Appendix) are related by the expression

$$I_2 = I_1 + 2Mb_c^2, \tag{B1}$$

where

$$M := \int \varrho_1(\bar{r}_1) d_{r_1}^3 = \int \varrho_2(\bar{r}_2) d_{r_2}^3 \tag{B2}$$

and b_c is the "width" of the convolution function, which is defined in ref. [3] by the expression

$$b_c^2 := \frac{1}{3}\langle r^2 \rangle_c. \tag{B3}$$

One way to establish the relationship (B1) is to note that

$$I = \int \varrho(\bar{r}) \cdot (x^2 + y^2) d_r^3 \tag{B4}$$

for an axis in the z-direction. This can be written

$$= \frac{2}{3} \int \varrho(\bar{s}) \cdot [r^2 - r^2 \cdot P_2(\hat{r})] d_r^3. \tag{B5}$$

Then

$$I_2 - I_1 = \frac{2}{3} \int r^2 \cdot [\varrho_1(\bar{r}) - \varrho_2(\bar{r})] d_r^3 \tag{B6}$$

where the terms on the right-hand side arising from the second term in the bracket in (B5) vanish because of the theorem relating moments established in Appendix A. The expression (B6) is simply

$$I_2 - I_1 = \frac{2}{3} M[\langle r^2 \rangle_2 - \langle r^2 \rangle_1], \tag{B7}$$

or

$$I_2 = I_1 + 2Mb_c^2, \tag{B8}$$

where we have made use of (B2), (B3) and the fact that $\langle r^2 \rangle_2 = \langle r^2 \rangle_1 + \langle r^2 \rangle_c$.
Another way to establish the relationship (B1) is to simply note that according to the "parallel axis theorem" of classical mechanics the contribution of each volume element in ϱ_2 to the moment of inertia is identical to the contribution from the same point for ϱ_1,

plus the mass times the moment of inertia of the convolution function about an axis through its center. Consequently,

$$I_2 = I_1 + M \cdot \frac{8\pi}{3} \int_0^\infty f_c(r) \cdot r^4 dr, \tag{B9}$$

where the second term on the right is simply $2Mb^2$ as before. For a Yukawa folding function

$$\begin{aligned} f_y(r) &= (4\pi a^3)^{-1} \cdot e^{-r/a}/(r/a), \\ b_y^2 &= 2a^2, \\ I_2 &= I_1 + 4Ma^2, \quad \text{(ref. 29)}. \end{aligned} \tag{B10}$$

For a Gaussian folding function

$$\begin{aligned} f_y(r) &= (\pi^{3/2}c^3)^{-1} \cdot e^{-(r/c)^2}, \\ b_y^2 &= c^2/2, \\ I_2 &= I_1 + Mc^2. \end{aligned} \tag{B11}$$

Note that, since the surface diffuseness b of a distribution generated from a sharp distribution by folding is identical to b_c (according to (30)), the moment of inertia of the diffuse system is independent of the functional form of the convolution function so long as its range is chosen to give the same value for b.

Received 15 September, 1975

REFERENCES

1. W. J. SWIATECKI: "The Energy of a Leptodermous System", private communication. C. F. Tsang, Ph.D. Thesis, UCRL-18899 (1969).
2. J. RANDRUP, W. J. SWIATECKI and C. F. TSANG: "Proximity Forces", LBL-3603, preliminary manuscript.
3. W. D. MYERS: "Geometrical Properties of Leptodermous Systems with Applications to Nuclei", *Nucl. Phys.*, A **204** 465 (1973).
4. G. SÜSSMANN: "Description of the Nuclear Surface by Moments", LBL-1615, May 1973.
5. H. J. KRAPPE and J. R. NIX: "Modified Definition of the Surface Energy in the Liquid-Drop Formula", Proceeding of the Third Symposium on the Physics and Chemistry of Fission, Rochester, August 1973.
6. W. GREINER: Proceedings of the Heavy-Ion Summer Study at Oak Ridge National Laboratory, June 1972.
7. K. A. BRUECKNER, J. R. BUCHLER, S. JORNA and R. J. LOMBARD: *Phys. Rev.*, **171**, 1188 (1968).
8. D. M. BRINK and N. ROWLEY: *Nucl. Phys.*, A **219**, 79 (1974).
9. R. A. BROGLIA and A. WINTER: *Phys. Reports*, **4**, 153 (1974).
10. J. WILCZYŃSKI: *Nucl. Phys.*, A **216**, 386 (1973).
11. R. BASS: *Phys. Lett.*, **47 B**, 139 (1973).
12. KENNETH W. FORD and JOHN G. WILLS: *Phys. Rev.*, **185** (1969) 1429.
13. G. W. GREENLESS, G. J. PYLE, and Y. C. TANG: *Phys. Rev.*, **171** (1968) 1115.
14. WILLIAM D. MYERS and W. J. SWIATECKI: *Ann. of Phys.*, (N. Y.) **55** (1969) 395
15. WILLIAM D. MYERS: *Phys. Letters*, **30 B** (1969) 451.
16. WILLIAM D. MYERS: *Nucl. Phys.*, A **145** (1970) 387.

17. A. S. TSAPIN: *Yad. Fiz.*, **1** (1965) 581; *Engl. transl.*: *Sov. J. Nucl. Phys.*, **1** (1965) 416.
18. A. R. BODMER: *Nucl. Phys.*, **17** (1960) 388.
19. H. R. COLLARD, L. R. B. ELTON, and R. HOFSTADTER: in *Nuclear Radii*, Vol. 2, Group I, Landolt-Börnstein, Numerical Data and Functional Relationships in Science and Technology (Springer-Verlag, Berlin, 1967)
20. L. R. B. ELTON: Nuclear Sizes (Oxford, 1961)
21. HAHN, RAVENHALL, and HOFSTADTER: *Phys. Rev.*, **101** (1956) 1131.
22. WILLIAM D. MYERS: "Droplet Model Description of Nuclear Masses, Fission Barriers and Radii", LBL-3428, November 1974.
23. M. P. FRICKE, E. E. GROSS, B. J. MORTON, and A. ZUCKER: *Phys. Rev.*, **156** (1967) 1207.
24. C. B. FULMER, J. B. BALL, A. SCOTT, and M. L. WHITEN: *Phys. Rev.*, **181** (1969) 1565.
25. SLANINA and MCMANUS: *Nucl. Phys.* **A 116** (1968) 271; Slanina, Ph.D. THESIS, Michigan State University (1969), unpublished.
26. OWEN and SATCHLER: *Comm. Nucl. Particle Phys.*, **5** (1972) 39.
27. L. W. OWEN and G. R. SATCHLER: "Multipole Moments of a Rounded Charge Distribution", *Nucl. Phys.*, **51**, 155 (1964).
28. Pointed out to me by N. ZELDES: see for example O. D. KELLOG: Foundations of Potential Theory, Springer-Verlag (1967).
29. This case was previously considered by J. R. Nix, private communication (June 1975).

W. D. Myers

WŁASNOŚCI GEOMETRYCZNE JĄDER

Streszczenie

Geometryczne własności jąder wyprowadzone są z kilku różnych źródeł. „Cienkoskóra" (leptodermous) natura rozkładu gęstości jądrowej oraz studni potencjału użyta jest dla powiązania różnych geometrycznych własności jąder i dla dostarczenia jednolitego sposobu ich opisu. Szeroko stosowane jest rozwinięcie własności radialnych w parametrze rozmycia powierzchni. Podane jest uzasadnienie stosowania splotu jako geometrycznego sposobu generowania rozkładów odpowiadających rozmytej powierzchni. Dostarcza on kilku uproszczeń o znaczeniu praktycznym.

В. Д. Майерс

ГЕОМЕТРИЧЕСКИЕ СВОЙСТВА ЯДЕР

Резюме

Геометрические свойства ядер выводится из нескольких различных источников. „Тонкокожистый" характер распределения ядерной плотности и потенциальной ямы используется, как связывающее звено различных геометрических свойств ядер, а также для получения унифицированного способа их описания. Широко применяется разложение радиальных свойств ядер по параметру размытия поверхности.

Излагается обоснование применения свертки, как геометрического метода генерирования распределений соответствующих размытой поверхности, дающего несколько упрощений практического характера.

TECHNICAL INFORMATION DIVISION
LAWRENCE BERKELEY LABORATORY
UNIVERSITY OF CALIFORNIA
BERKELEY, CALIFORNIA 94720